# Liquid Plasma Crystals on the International Space Station

E. Gehr,* A. Terrell,† B. Andrew,‡ E. G. Kostadinova,§ L. S. Matthews,¶ and T. W. Hyde‖
*Center for Astrophysics, Space Physics, and Engineering Research and Department of Physics, Baylor University, TX, USA*
*Department of Physics, Auburn University, AL, USA*

**This study examines the structure and stability of filamentary dusty plasmas using data from the Plasmakristall-4 (PK-4) facility on board the International Space Station. Under the action of a polarity-switched DC electric field, the dust particles in the PK-4 discharge have been found to organize into field-aligned extended filaments, which has been compared to the filamentary state in electrorheological (ER) fluids. Here we discuss how, in addition to an ER-type structural transition, the PK-4 dusty plasmas exhibit structural states reminiscent of those observed in liquid crystals (LCs) with rod-shaped molecules. We find that dust particles within the filaments are strongly coupled in a crystalline-like structure, while the coupling of particles across filaments is liquid-like. In addition to a common orientation along a director axis (nematic behavior), the dust filaments also appear to align in large-scale nested structures, or shells (smectic behavior). Finally, these filaments are found to further arrange in hexagonal patterns within the plane orthogonal to the director axis, suggesting the possibility for smectic-B and smectic-C structural states. As the observed ER and LC features of the filamentary dusty plasma states are sensitive to variations in the PK-4 discharge conditions, we argue that these dusty plasmas can provide a controlled analogous system for the study of fundamental phenomena in soft matter, such as the origins of pattern formation and universality of phase transitions.**

## I. Nomenclature

| | | |
|---|---|---|
| $r$ | = | spherical radius |
| $\theta$ | = | azimuthal angle $\{-\pi/2, \pi/2\}$ |
| $\phi$ | = | polar angle $[0, 2\pi\}$ |
| $g(r)$ | = | pair correlation function for two-dimensional data |
| $G(r, \theta, \phi)$ | = | pair correlation function for three-dimensional data |
| $G_\phi(r, \theta)$ | = | pair correlation function integrated over all $\phi$'s |
| $G_\theta(r, \phi)$ | = | pair correlation function integrated over all $\theta$'s |

## II. Introduction

Materials in the liquid crystal (LC) state of matter exhibit properties of both conventional liquids and solids. Beyond their well-known use in LC displays [1], [2], liquid crystals can potentially transform technology and medicine through the development of soft robotics [3], [4], artificial muscles [5], [6], and LC polymers [7], [8], [9]. Liquid crystals are also known to exhibit the electrorheological effect (change of viscosity due to electric-field-induced structural transition) [10], [11], [12], which expands their application to the development of fast clutches and hydraulic valves, brakes, and shock absorbers [13], [14], [15]. The successful utilization of LCs in all these applications relies on controlled self-assembly and transitions into different LC phases. Microscopic experimental treatment of liquid crystals is challenging due to their high material density, the presence of strong interactions, and the effect of many-body

*Undergraduate Student Researcher, Department of Physics, Baylor University, Waco, TX, USA
†Undergraduate Student Researcher, Department of Physics, Baylor University, Waco, TX, USA
‡Graduate Student Researcher, Department of Physics, Auburn University, Auburn, AL, USA
§Assistant Professor, Department of Physics, Auburn University, Auburn, AL, USA
¶Professor, Department of Physics, Baylor University, Waco, TX, USA
‖Professor, Department of Physics, Baylor University, Waco, TX, USA

correlations. One approach to the study of LC phenomena is the use of microgravity complex (dusty) plasma analogues, which consist of charged micron-sized particles suspended in weakly-ionized gas.

Dust grains immersed in plasma become negatively charged and are subject to both ion drag forces and collective interactions. As the magnitude of the dust charge depends on both on the dust location in the plasma (e.g., plasma sheath or bulk plasma) and on the time evolution of the plasma conditions, the coupling strength among dust particles in complex plasmas can vary in a wide range, resulting in the formation of diverse structural states. Dusty plasmas can self-organize into strongly coupled fluids and crystalline structures [16], [17], [18], [19], which makes them ideal for the study of self-organization and stability, phase transitions, and transport phenomena. On Earth, the liquid crystal properties of dusty plasmas have been demonstrated in experiments with elongated dust particles in capacitively coupled RF discharges [20], [21] and cylindrical dust particles in DC discharges [22], [23]. The discovery of the electrorheological effect in microgravity dusty plasma demonstrated that dusty plasmas can successfully be used as an analogue for the study of phase transitions in 'smart' materials [24], [25], [26]. However, unlike conventional electrorheological fluids, where the transition to a filamentary state is induced by polarization of the grains themselves, in electrorheological plasmas, effective polarization is caused by the dust interaction with the ion flow. Specifically, streaming ions are deflected and focused by a negatively charged dust grain, which results in the formation of ion wakefield downstream from the grain.

The first electrorheological (ER) complex plasma was observed in the Plasmakristall-3 (PK-3) Plus setup [27] on board the ISS. The interaction potential guiding the ER effect in PK-3 Plus was proposed to have a dipole-dipole form, which seemed to yield agreement between MD simulations and experiments [25]. After the first observation of filamentary structures in the PK-4 DC discharge, it was conjectured that the interparticle interaction in this setup possibly has a similar dipole-dipole form [25], [28], [29]. However, recent numerical simulations [30], [31] reveal that the formation of filamentary structures in PK-4 is guided by a more complex interaction potential resulting from the interplay between the polarity switched DC electric field and the onset of high-frequency ionization waves present in the PK-4 discharge [32]. Several studies have suggested that, in addition to the electrorheological effect, the PK-4 filamentary structures exhibit simultaneous liquid and crystalline properties in a broad range of experimental conditions [33], [34], [35], [36]. Moreover, parabolic flight experiments and molecular dynamics simulations of dusty plasmas in the PK-4 setup have confirmed that the dust filaments can arrange in hexagonal patterns and form distinct layers [37], [38] which are properties observed in liquid crystals. Thus, it can be argued that the PK-4 filamentary dusty plasmas are unique structures that combine properties of both electrorheological fluids and liquid crystals.

Here we investigate the simultaneous liquid and crystalline properties of dusty plasma clouds using video data from the experimental facility Plasma Kristall-4 (PK-4) on board the International Space Station [39]. Unlike molecular liquid crystals, complex plasmas are optically thin and macroscopic, which allows for the real-time observation of particle dynamics at the kinetic level. For each set of experimental conditions, particle tracking is used to obtain dust positions as a function of time. Then, the structural propertied of the dust clouds are assessed by calculating various pair correlation functions. The computed coupling of dust particles within filaments, across filaments in a plane, and across the bulk structure are then used to identify properties reminiscent to those observed in the nematic and smectic phases of conventional LCs.

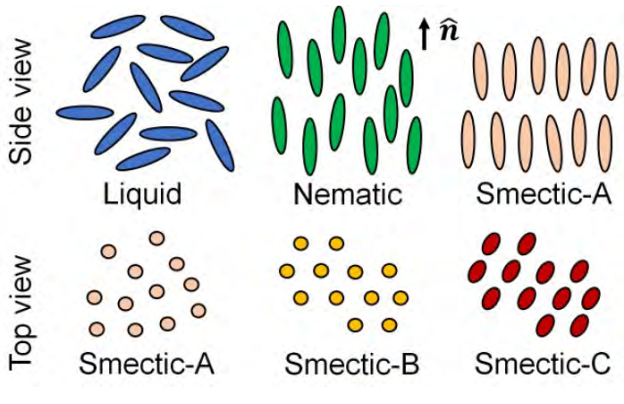


**Fig. 1 Patterns and order observed in LC phases**

In the liquid-nematic phase transition, the LC molecules align along a preferred direction $\hat{n}$, while in the nematic-smectic-A transition, the molecules additionally arrange in layers. In the smectic-B phase, as well as several other smectic phases, hexagonal patterns form within the ordered layers (Fig. 1). Understanding and controlling pattern formation in various nematic-smectic transitions will enable promising methods for fast and affordable fabrication of optical microarrays [40], [41] and assembly of functional nanoparticles [42], [43]. The structural analysis of the PK-4 dusty plasmas reveals that dust particles within the same filament are strongly coupled in a crystalline-like structure, while the coupling of particles across filaments is liquid-like. Therefore, the filamentary state of these structures is intermediate between a liquid and a crystal. In addition to common orientation along a director axis, typical for a nematic state, the dust filaments are observed to align in nested shells,

suggesting smectic behavior. Calculating a three-dimensional (3D) pair correlation function reveals that the filaments also align in hexagonal patterns in the plane perpendicular to the director axis, which is typical for smectic-B and smectic-C states.

An important distinction between PK-4 dusty plasmas and conventional LCs is the presence of external electric field needed to establish the interaction potential leading to the formation of filaments. This is why previous investigations of the filamentary dusty plasma state have used an analogy with ER fluids instead of LCs. However, our analysis of PK-4 data indicates that the presence of external electric field alone in insufficient to establish the observed filament alignment, layering and, patter formation. Instead, the dust-dust interaction potential resulting from the presence of external electric field can be viewed as analogous to the interatomic interaction potentials bonding atoms in rod-shaped molecules in conventional LCs. An additional necessary condition for the formation of different filamentary states in dusty plasma is sufficient neutral gas pressure. In dusty plasmas, increasing pressure can be used to minimize dust diffusion through collisions with neutral particles, thus "cooling down" the dust cloud. In other words, within a certain gas pressure range (yielding good ionization rates for a given power supply), pressure has the role of inverse temperature. We observe that in PK-4, the dust filaments stabilize at higher pressures, which is analogous to lowering temperature in experiments with conventional LCs. Thus, it is likely that the dusty plasmas discussed here exhibit properties intermediate between ER fluids and LCs or properties characteristics of LCs that exhibit the ER effect.

## III. PK-4 Experimental Setup

The PK-4 laboratory is a successor of the PKE-Nefedov [44] and PK-3 Plus [27]. The PK-4 experimental setup consists of an elongated Π-shaped glass chamber (85 cm length and 3 cm inner diameter) in which the plasma can be ignited either by cylindrical DC electrodes or by RF coils (Fig. 2a). In this paper, we focus on the behavior of dusty plasma in the experiments utilizing the pure DC discharge regime. A bipolar, high-voltage power supply powers the DC electrodes and provides output current as high as 3.1 mA and a maximum voltage of 2.7 kV. The DC current can either be unidirectional or polarity-switched, which is used to transport dust after injection or to trap/manipulate dust, respectively. The dust particles are illuminated by a laser sheet (532 nm diode laser) and video data is collected with two identical particle observation (PO) video cameras (1600 × 1200-pixel CCD chips).

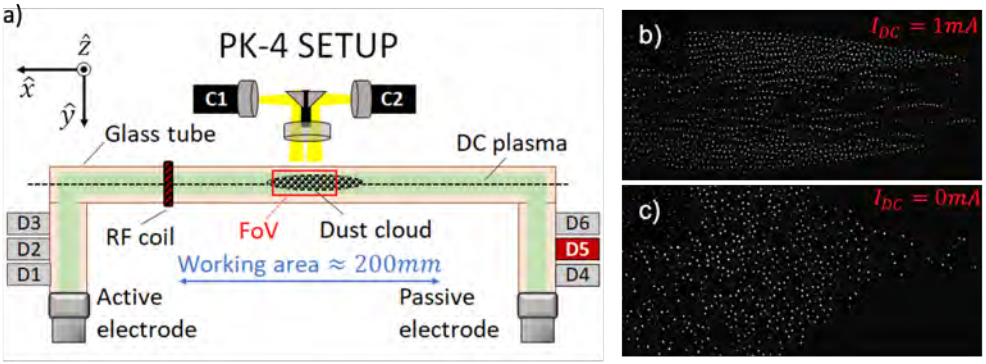


**Fig. 2 a) The PK-4 setup: DC plasma is created in a Π-shaped glass chamber. Dust particles are injected from one of six dispensers (D1-D6). Laser illumination (not shown) and video cameras are used to observe the dust cloud in the field of view (FoV). b) Filamentary dusty plasma induced from the application of DC current. c) Isotropic dusty plasma in the absence of DC current.**

All experiments analyzed in this paper were recorded at frame rate of 71.4 fps for each PO camera, which yields a combined field of view (FoV) ≈ 44 × 7 mm$^2$ (assuming resolution of 14 × 14 $\mu m^2$/px). In addition, the characteristics of the plasma discharge were monitored by a plasma glow observation (PGO) camera (640 × 480-pixel CCD chip) which covers the entire working area of the experiment with a resolution of ≈ 430 × 430 $\mu m^2$/px. The frame rate for the images obtained with the PGO camera is 15.2 fps .

The experiments described in this paper were conducted on July 26, 2019, as part of PK-4 ISS Campaign 7. We focus on experiments in neon DC plasma at pressures approximately equal to 28.5 Pa, 46.1 Pa, and 70.5 Pa. The dust particles introduced to the plasma were melamine-formaldehyde (MF) spheres of diameter 3.38 ± 0.07 $\mu m$. For each pressure level, the micro-particles were injected and transported to the FoV by a unidirectional DC field at 1 mA. Then,

the dust particles were trapped in a cloud formation using polarity switching of the DC current with 500 Hz frequency and 50% duty cycle. The frequency response of micron-sized particles, a function of the charge-to-mass ratio, is usually in the range of 10-100 Hz [45], [46]. Therefore, the dust has negligible response to the polarity switching frequency of 500 Hz, instead, the dust particles are subject to a time-averaged electric field. With the symmetric duty cycle (50%) the magnitude of this average field is zero. If an asymmetric duty cycle is used, the dust experiences a net electric force, causing the dust cloud to move along the axis of the glass chamber. However, since the plasma species respond to a 500 Hz frequency, an indirect dust response to the polarity switching produced by plasma-dust interactions is possible and will be discussed in the coming sections.

## IV. Evidence of Simultaneous Liquid and Crystalline Properties

When the DC current in PK-4 is increased from zero, the induced electric field causes the dusty plasma cloud to transition from an isotropic (liquid-like) state to a state where the dust particles form filaments aligned along the direction $\hat{n}$ of the electric field (Fig. 2b, c). The filamentary effect is enhanced by switching the polarity of the electric field with a frequency higher than the dust response frequency ($\geq$ 100 Hz). When the duty cycle of the polarity switching is chosen to be symmetric, symmetric ion wakefields are expected to form around each dust grain (Fig. 3). However, the duty cycle can be tuned to cause asymmetries, which in turn modulate the dust interactions and the resulting filamentary structure [26]. An analogy with liquid crystals is recognized by considering a dust particle filament as an equivalent of a LC rod-shaped molecule. Note that this is different from liquid crystal properties reported in complex plasma experiments with cylindrical dust particles [20], [23].

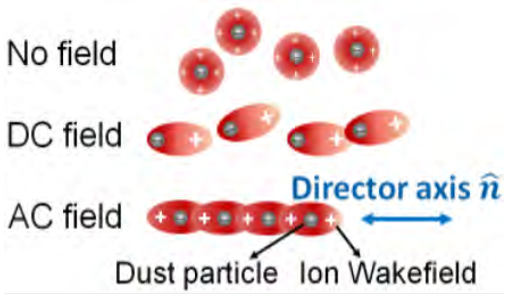


**Fig. 3 Formation of dusty plasma "rod-shaped molecules" under the action of external electric field.**

Fig. 4a depicts an image of a typical filamentary dust cloud in neon plasma at pressure 70.5 Pa and DC current 0.7 mA. These conditions yield extended filamentary structures, consisting of 20-30 particles each (Fig. 4b). In Fig. 4c, we show the particle trajectories over a period of $\sim$ 1.5 seconds (camera frame rate 71.4 frames per second) in a small region of the cloud (highlighted by a white rectangle in Fig. 4a). The trajectories indicate that as dust particles move, they remain trapped in the filamentary structures, suggesting strong coupling. In addition, similar to rod-shaped molecules in the nematic LC phase, the dust filaments exhibit common orientation along a director axis, which coincides with the direction of the externally applied electric field.

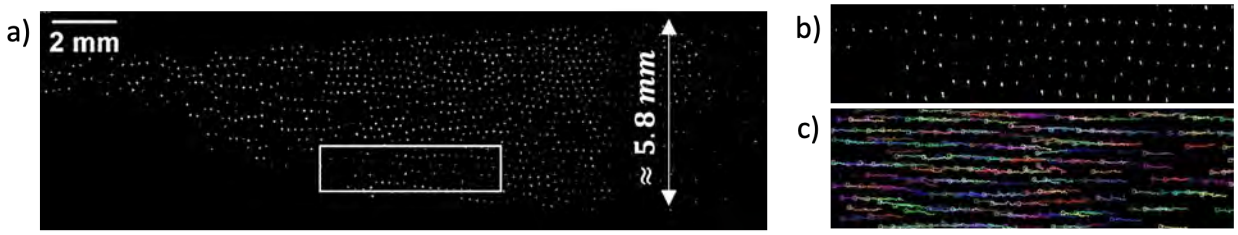


**Fig. 4 a) Filamentary dusty plasma cloud in neon DC discharge with polarity-switched electric field. b) Zoomed in section of the cloud showing filamentary structure. c) Trajectories of particles within the cloud over $\approx$ 1.5 s period. Data from PK-4 experiment with pressure 70.5 Pa and DC current 0.7 mA.**

The liquid crystal properties of filamentary dusty plasmas in the PK-4 experiment are also assessed from calculating the pair correlation function $g(r)$, which quantifies the probability to find another particle as a function of distance from a reference particle. If the $g(r)$ function exhibits sharp peaks at periodic distances and troughs dropping to zero in-between peaks, the underlying structure is crystalline. For a liquid-like structure, the peaks are less pronounced, and the troughs do not drop to zero. The average interparticle separation is generally defined as the distance at which the first peak of $g(r)$ occurs. Shifts in the location of this peak can suggest changes in dust density and the existence of layers throughout the cloud. A (normalized) pair correlation function for particles within a dust filament is shown in Fig. 5a. Fig. 5a shows the (normalized) pair correlation function calculated for particles within dusty plasma filaments.

The $g(r)$ plot for these particles exhibits well-defined peaks at periodic distances, indicating a crystalline structure of the filaments. In contrast, the $g(r)$ calculated for particles within the 2D plane suggests liquid-like state (Fig. 5b). Similar to the asymmetric interactions found in LCs, here we find strong (crystal-like) coupling among the grains within individual filaments and weaker (liquid-like) coupling across filaments within a plane.

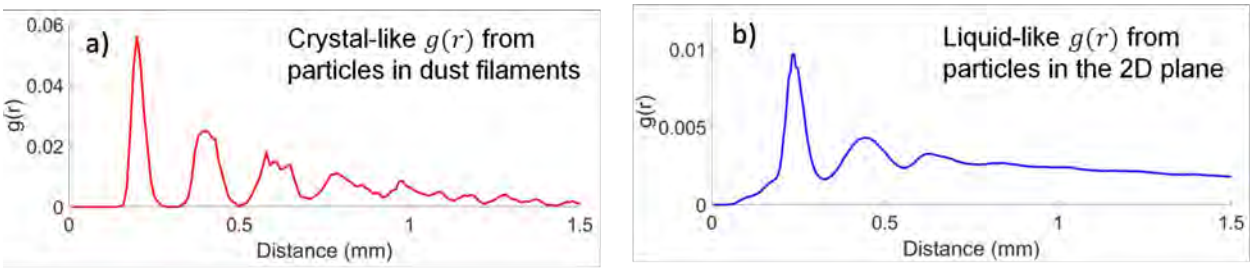


**Fig. 5 Pair correlation function $g(r)$ for a) particles within dust filaments and b) particles within the 2D plane. Data from PK-4 experiment with pressure 70.5 Pa and DC current 0.7 mA.**

In addition to common orientation along a director axis (nematic behavior), the dusty plasma filaments also appear to align in large-scale layers, or shells (smectic behavior). This is visible from an abrupt change in the pair correlation function as one considers particles in different regions of the cloud. Typically, the illumination laser sheet and particle observation cameras are located at a fixed position on the $\hat{y}$-axis and provide 2D images of the dust structure in the $\hat{x}$-$\hat{z}$ plane (Fig. 2a). During a "Y-scan" procedure, the laser sheet and cameras are moved along the $\hat{y}$-axis with a constant speed, providing a succession of 2D images of the dust structure, otherwise in or out of the FoV. Fig. 6 shows the $g(r)$ function calculated for particles from successive 2D planes, starting at the center of the cloud (red plots) and moving toward its exterior (dark yellow plots). The location of the first peak in each plot suggests the average interparticle separation for the dust grains in the corresponding 2D plane. For particles located within a central region of the cloud (red plots), the interparticle separation is $\approx 260\ \mu m$. For particles in a 2D plane located 2 $mm$ away from the central region (blue plots), the interparticle separation decreases to $\approx 220\ \mu m$. For particles in a plane located 4 $mm$ away from the central region, the shape of the $g(r)$ function and the location of the first peak change abruptly, yielding an interparticle separation of $\approx 85\ \mu m$. This indicates that a large dust density gradient occurs the region between 2 $mm$ and 4 $mm$ away from the center of the cloud, suggesting a layered structure.

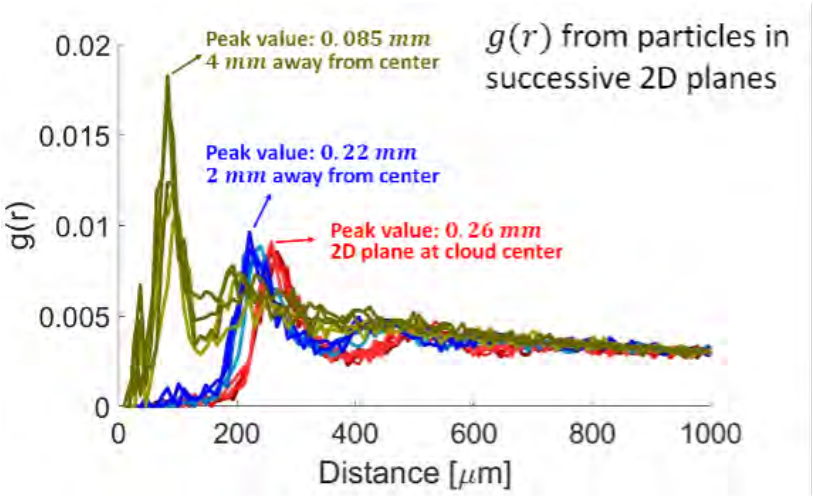


**Fig. 6 Pair correlation function $g(r)$ for dust particles within successive 2D planes. Data was obtained from a laser sheet scan starting from the cloud exterior (olive green shades) to the cloud center (red shades). Different shades indicate 2D planes at increasing locations away from the cloud exterior. Data is presented for 1 mA DC current and pressure 46 Pa.**

The layer formation is confirmed from examination of video data obtained for the same experiment during a Y-scan

procedure. Fig. 7 shows successive video frames obtained as the laser sheet illumination moves from the center to the exterior of the cloud. These images reveal the presence of a particle-free gap separating two layered structures, suggesting that the dust cloud consists of at least two nested spheroids. These results give us confidence that microgravity dusty plasmas area suitable test system for investigating the universal characteristics of liquid crystals in both nematic and smectic phases.

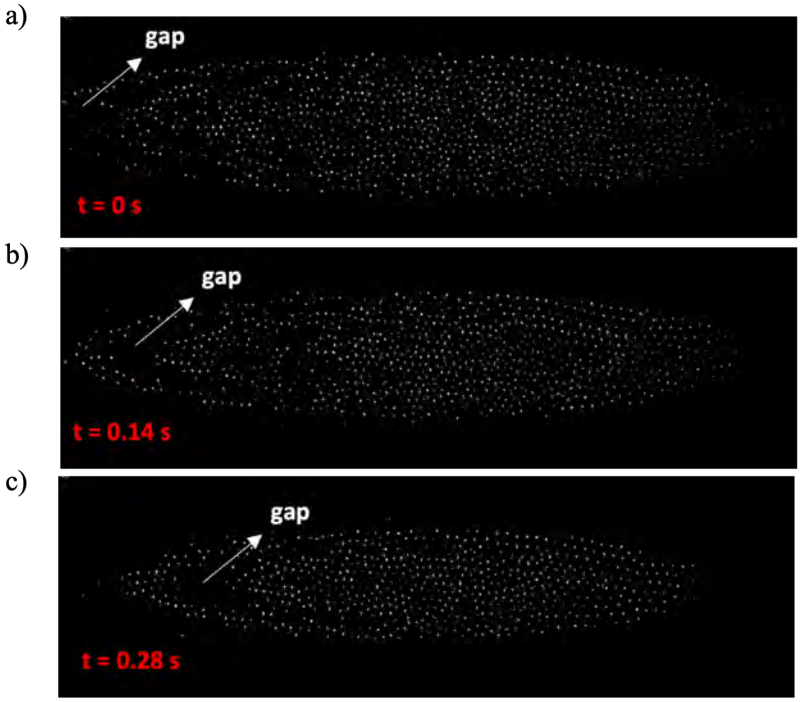


**Fig. 7 Successive images of the dust cloud taken 0.14 s apart during a Y-scan with a particle observation laser sheet (laser current 0.7 A and scan velocity 1 mm/s). Data is presented for 1 mA DC current and pressure 46 Pa. The approximate laser offset from its initial position at the center of the discharge tube is a) 2.68 mm, b) 2.82 mm, and c) 2.96 mm. The images were recorded with a single PO camera with a FoV $\approx 22.6 \times 6.8$ mm$^2$. As time increases and the PO laser moves away from the central axis, clear gaps (void of particles) are observed on the left side of the cloud. The gap seems to separate distinct particle structures.**

## V. Data Collection And Three-Dimensional Pair Correlation Function

Two types of videos were analyzed: (i) videos where the cameras laser sheet were fixed in the central region of the cloud and (ii) videos from Y-scan procedures, where the cameras and laser sheet were moved across the cloud. Here we primarily focus on videos from the Y-scan procedures, which allow for the study of the three-dimensional structure. The particle positions as a function of time were obtained using the particle tracking MOSAICsuite plugin of Fiji, which is a distribution of ImageJ. The locations of the detected particles in each (two-dimensional) video frame is then converted into position in physical space using pixel resolution of 14.20 $\mu$m [39]. The third dimension of the dust particle positions is determined using the known constant speed of the laser scan of 1.0 mm/s and the video frame rate of 71.4 fps, leading to a displacement of about 14 $\mu$m between frames. As the laser sheet scans through the cloud, some particles may be picked up in multiple, consecutive frames. To assure that our analysis does not double count particles, we filter out particles that are less than a threshold distance from another particle in the next few subsequent frames. This process yields a three-dimensional representation of the dust cloud, shown in Fig. 8. Fig. 8b, shows an end-view of the dust cloud looking down along the director axis. The presence of cylindrical shells can be seen on the right side of the image. The 3D dust positions are used to perform structural analysis on the overall cloud which is relatively stable over the duration of the Y-scan.

The three-dimensional coordinates obtained form the reconstructed dust cloud allow for the calculation of a

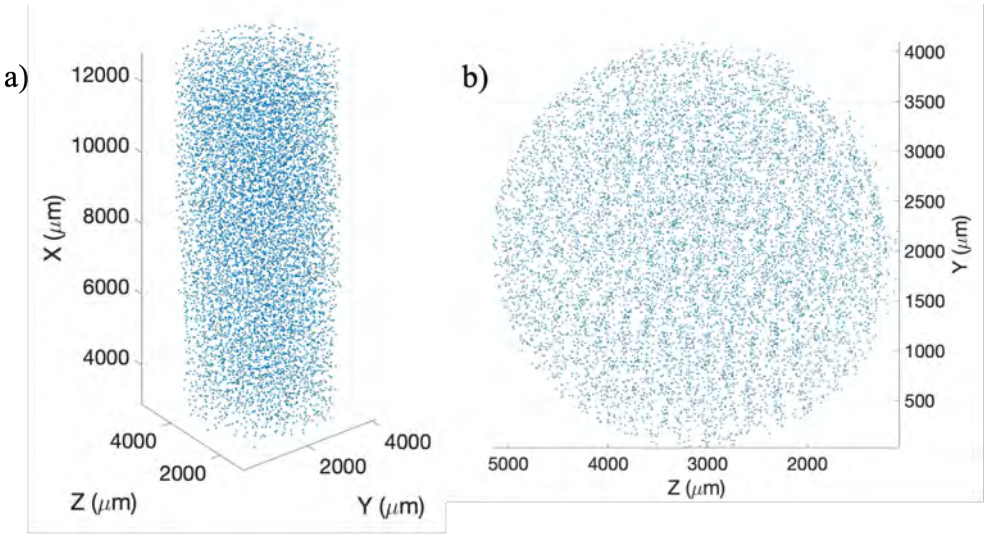


**Fig. 8 Cylindrical dust cloud at 28.5 Pa and 0.7 mA reconstructed from particle position data obtained through Fiji's MOSAICsuite particle tracking software showing a) a side view and b) a top view.**

three-dimensional pair correlation function in spherical coordinates [34], [35]

$$G(r,\theta,\phi) = \frac{1}{n_d N} \sum_{i,j=1,i\neq j}^{N} \frac{\delta(r_{ij}-r)\delta(\theta_{ij}-\theta)\delta(\phi_{ij}-\phi)}{4\pi r^2\cos(\theta)} \tag{1}$$

where $i$ and $j$ are particle indices and $r_{ij}$, $\theta_{ij}$, and $\phi_{ij}$ are the magnitude, the azimuthal angle, and the polar angle, respectively, of the vector connecting two particles $i$ and $j$ as illustrated in Fig. 9. The $\delta$ functions represent binning the data in all three dimensions. $G(r,\theta,\phi)$ is used to identify the formation of filaments, patterns, layered structures in the three-dimensional cloud structure. In order to graphically represent the data collected by $G(r,\theta,\phi)$, the two-dimensional probability distributions $G_\phi(r,\theta)$ and $G_\theta(r,\phi)$ are obtained by integrating over each of the angles, with

$$G_\phi(r,\theta) = \int_0^{2\pi} G(r,\theta,\phi)d\phi \tag{2}$$

$$G_\theta(r,\phi) = \int_{-\frac{\pi}{2}}^{\frac{\pi}{2}} G(r,\theta,\phi)\cos(\theta)d\theta. \tag{3}$$

The polar angle $\theta$ ranges from $\{-\pi/2, \pi/2\}$ radians, with $\theta = 0$ on the yz-plane (Fig. 9a). Particles within a given filament aligned with the director axis will be located at $\theta \approx \pm\pi/2$. At intermediate angles of $\theta$, characteristics of nearby filaments become apparent. The polar angle $\phi$ takes values in the range $\{0, 2\pi\}$ radians with $\phi = 0$ on the xy-plane (Fig. 9b). The angle $\phi$ gives information about the location of neighboring filaments, revealing characteristics of the layered structure. Depending on the values of experimental parameters (i.e. pressure, current), the layered structure is more pronounced and hexagonal symmetry becomes apparent.

## VI. Structural Analysis

Fig. 10 displays the 2D pair correlation function $G_\phi(r,\theta)$ and Fig. 11 shows the 2D pair correlation function $G_\theta(r,\phi)$ for dust clouds at three different pressures $P$ = 28.5 Pa, 46.1 Pa, and 70.5 Pa, respectively, with the discharge current set at 0.7 mA.

In Fig. 10, the bright spots for small $r$ centered about $\theta = 0$ are artifacts of the laser scan, as the particles in the dust clouds are not completely stationary. The periodic bright spots for distinct radial distances at $\theta = \pm\pi/2$ are referred to as as "string peaks" [34] and indicate the order within the filaments. The value of $r$ for the first string peak gives the average interparticle separation. At higher pressure, the string peaks are more pronounced at larger $r$ indicating increased order within a filament. Intermediate angles of $\theta$, reveal arch-like structures in the pair correlation plots.

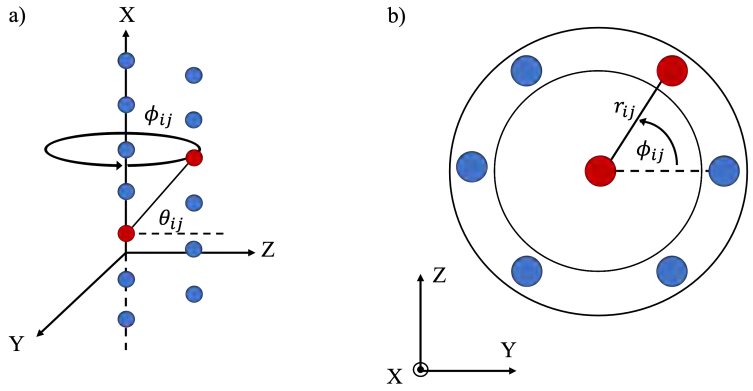


**Fig. 9 Coordinate system used for three-dimensional pair correlation functions expressed through a) a side view and b) a top view of the cloud.**

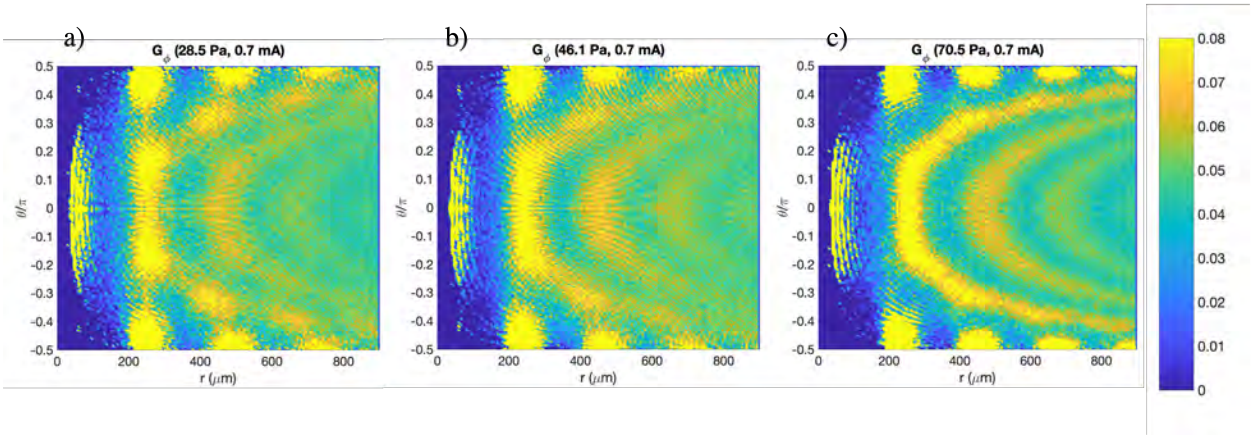


**Fig. 10 Plots of $G_\phi(r,\theta)$ for three different pressures: a) 28.5 Pa, b) 46.1 Pa, and c) 70.5 Pa.**

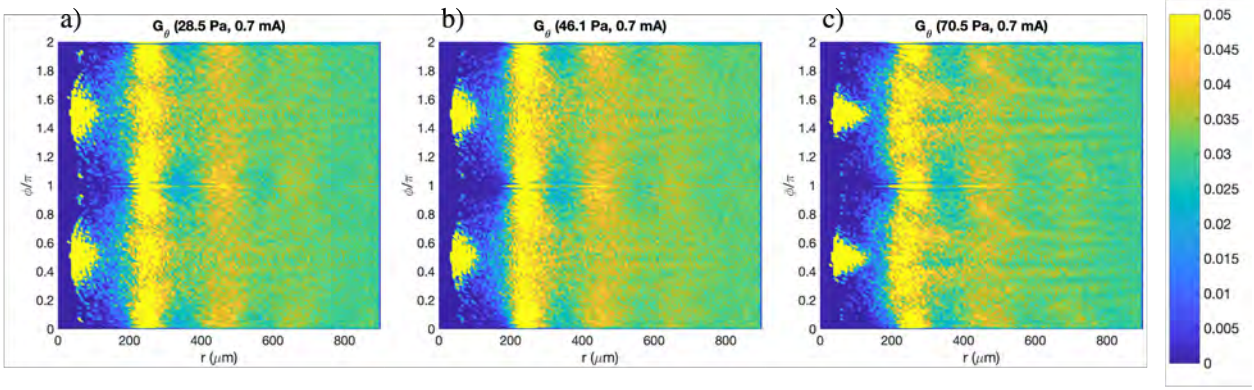


**Fig. 11 Plots of $G_\theta(r,\phi)$ for three different pressures: a) 28.5 Pa, b) 46.1 Pa, and c) 70.5 Pa. Each plot corresponds to the same cloud represented by $G_\phi(r,\theta)$ in Fig. 10.**

At lower pressures, these arches have distinct peaks within them, which indicates that the particles in neighboring chains are off-set from each other with fixed interparticle spacing, indicating strong coupling between neighboring filaments. As the pressure increases, the arches smooth out and the discernible pockets of high probability are no longer visible, suggesting that the filaments at higher pressures have more freedom in their location along the director axis

relative to other filaments. Thus, from Fig. 10 we see that at higher pressures, the order within filaments improves (crystalline behavior), while their degree of freedom to move with respect to each other increases (liquid behavior). This is analogous to the behavior expected for rod-like particles in the liquid-nematic phase of LCs (Fig. 1).

Further information about the layered structure of the cloud is obtained from $G_\theta(r,\phi)$ as shown in Fig. 11. The evenly spaced band-like structure of high probability regions is related to the interparticle spacing within each filament. At the lowest pressure of 28.5 Pa (Fig. 11a), the first, brightest band reveals six identifiable regions (brighter blobs) of high probability, suggesting the presence of a hexagonal structure about the reference particle. As the pressure increases, the hexagonal symmetry is less distinct. At the highest pressure, the primary band is no longer straight, but exhibits wave-like shape showing that the particles in adjacent filaments are not aligned in the same plane. Interestingly, the striations appear in the band at distinct angles at larger interparticle separations. This suggests that there is a transition from the interior to the exterior of the cloud. At the cloud's interior, the low correlation indicates that the filaments are able to move freely with respect to each other. The filaments at the exterior of the cloud exhibit a stronger coupling and less freedom to move with respect to each other.

## VII. Average Interparticle Separation

We also analyzed data from dust particles within a central plane of the dust cloud for periods when no Y-scan is taking place (therefore, most of the dust particles remain in the field of view for the entire image sequence.) Fig. 12 depicts the calculated $g(r)$ for each frame plotted over each other where the colors indicate the progression of time (Fig. 12a,c). The time-averaged pair correlation functions are shown in Fig. 12b,d. The 2D pair correlation plots, yield similar average interparticle separation as the 3D pair correlation plots from Fig. 10 and Fig. 11. This validates the assumption that the cloud is largely stationary during the Y-scan and that the stacked images capture the clouds' 3D structure. The average interparticle spacing decreases slightly as the pressure is increased. Note that at the lower pressure (Fig. 12b) there are four distinct peaks. In contrast, the 2D pair correlation at high pressure (Fig. 12d) has more pronounced peaks at the first and second interparticle separation distances, but only three peaks are clearly distinguishable. This is another indication that at the higher pressure, the dust particles are strongly coupled within the filaments but the coupling across filaments is liquid-like.

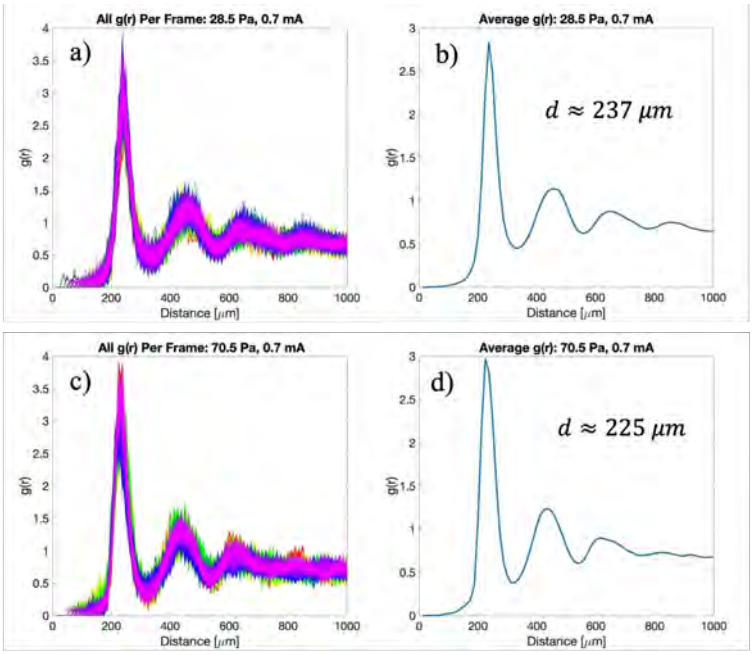


**Fig. 12 Pair correlation function $g(r)$ calculated for paricles within 2D central planes of the dust clouds at a),b) 28.5 Pa and c),d) 70.5 Pa. The colors in a) and c) indicate the each frame of the video sequence and the corresponding time-averaged pair correlation functions are shown in b) and d). The location of the primary peak gives the average interparticle spacing in the cloud, as indicated on the plots.**

## VIII. Conclusion

Here we presented analysis of dusty plasma experiments from the PK-4 facility on board the International Space Station. Due to the polarity-switched electric field in the PK-4 DC discharge, the dusty plasmas are observed to organize into field-aligned filaments. It has been suggested that this filamentary dusty plasma state is reminiscent of the electrorheological state observed in smart materials. While the external electric field is certainly important for establishing the interaction potential needed for the formation of dust filaments, the resulting dusty plasma clouds exhibit rich structural behavior, which is sensitive to gas pressure in the discharge. Specifically, we observe that, in addition to common orientation along the direction of the electric field, the filaments in PK-4 can also exhibit pressure-dependent pattern formation and layering, which are characteristic of the nematic and the various smectic states of liquid crystals. Based on these initial observations, we propose that microgravity dusty plasma experiments can be used as a macroscopic analogue system for the study of fundamental quastions in the theory of liquid crystals, such as the universality of LC phase transitions, the origins of pattern formation, and the propagation of defects a critical conditions.

The similarity between the dusty plasma filamentary state and different features of LCs was estaablished using several methods. Particle tracking data was used to obtain the pair correlation functions for particles within individual filaments, particles across filaments within a 2D central plane, and particles within the 3D volume of the cloud. For all examined pressure cases, it was established that the particles within the filaments exhibit crystalline-like coupling, while particles across filaments exhibit weaker coupling. However, increasing the pressure results in improving crystallinity within the filaments and enhancing the liquid-like coupling across filaments. Thus, we conclude that for a fixed electric field, increased pressure results in a structural state reminiscent of the nematic state in liquid crystals. At lower pressures, the dust particles within filaments still exhibit crystalline-like coupling but the increased coupling strength among filaments leads to their arrangement in hexagonal patterns.

Analysis of video data obtained during a laser scan across the entire dust clouds revealed that for certain pressure-current conditions, the dust filaments are arranged in at least two nested spheroid layers with distinct coupling and interparticle separations. The preliminary evidence of layering and formation of hexagonal patterns suggest that the PK-4 dusty plasmas can also exhibit structural states reminiscent of the smectic phases in conventional LCs. Additional insight into the transition between the different structural states within the dust cloud can be gained from numerical modeling of the plasma discharge coupled with simulations of the dust charging and dynamics. The difference in dust coupling seen within filaments and across filaments is largely due to the asymmetric interaction potentials between the dust grains due to the focusing of the ions in "ion wakes" downstream of the grains [30], [31]. Future work will focus on correlating the dynamic discharge conditions, which occur on very fast time scales [32] to the dust dynamics, which respond on slower time scales.

## Acknowledgments

This material is based on work supported by NSF grant numbers 1903450 and 1740203, NASA grant number 1571701, and US Department of Energy, Office of Science, Office of Fusion Energy Sciences under award number DE-SC0021334. All authors gratefully acknowledge the joint ESA - Roscosmos "Experiment Plasmakristall-4" onboard the International Space Station. The microgravity research is funded by the space administration of the Deutsches Zentrum für Luft- und Raumfahrt eV with funds from the federal ministry for economy and technology according to a resolution of the Deutscher Bundestag under Grants No. 50WM1441 and No. 50WM2044.

## References

[1] Chen, H.-W., Lee, J.-H., Lin, B.-Y., Chen, S., and Wu, S.-T., "Liquid crystal display and organic light-emitting diode display: present status and future perspectives," *Light: Science & Applications*, Vol. 7, No. 3, 2018, pp. 17168–17168. https://doi.org/10.1038/lsa.2017.168, URL https://www.nature.com/articles/lsa2017168/, number: 3 Publisher: Nature Publishing Group.

[2] White, D. L., and Taylor, G. N., "New absorptive mode reflective liquid-crystal display device," *Journal of Applied Physics*, Vol. 45, No. 11, 1974, pp. 4718–4723. https://doi.org/10.1063/1.1663124, URL https://aip.scitation.org/doi/10.1063/1.1663124, publisher: American Institute of Physics.

[3] Lv, P., Yang, X., Bisoyi, H. K., Zeng, H., Zhang, X., Chen, Y., Xue, P., Shi, S., Priimagi, A., Wang, L., Feng, W., and Li, Q., "Stimulus-driven liquid metal and liquid crystal network actuators for programmable soft robotics," *Materials Horizons*, Vol. 8, No. 9, 2021, pp. 2475–2484. https://doi.org/10.1039/d1mh00623a.

[4] Shen, Z., Chen, F., Zhu, X., Yong, K.-T., and Gu, G., "Stimuli-responsive functional materials for soft robotics," *Journal of Materials Chemistry B*, Vol. 8, No. 39, 2020, pp. 8972–8991. https://doi.org/10.1039/D0TB01585G, URL https://pubs.rsc.org/en/content/articlelanding/2020/tb/d0tb01585g, publisher: The Royal Society of Chemistry.

[5] Li, M.-H., and Keller, P., "Artificial muscles based on liquid crystal elastomers," *Philosophical Transactions. Series A, Mathematical, Physical, and Engineering Sciences*, Vol. 364, No. 1847, 2006, pp. 2763–2777. https://doi.org/10.1098/rsta.2006.1853.

[6] Buguin, A., Li, M.-H., Silberzan, P., Ladoux, B., and Keller, P., "Micro-actuators: when artificial muscles made of nematic liquid crystal elastomers meet soft lithography," *Journal of the American Chemical Society*, Vol. 128, No. 4, 2006, pp. 1088–1089. https://doi.org/10.1021/ja0575070.

[7] Liu, X., Debije, M. G., Heuts, J. P. A., and Schenning, A. P. H. J., "Liquid-Crystalline Polymer Particles Prepared by Classical Polymerization Techniques," *Chemistry (Weinheim an Der Bergstrasse, Germany)*, Vol. 27, No. 57, 2021, pp. 14168–14178. https://doi.org/10.1002/chem.202102224.

[8] Collyer, A. A. (ed.), *Liquid Crystal Polymers: From Structures to Applications*, Springer Netherlands, Dordrecht, 1993. https://doi.org/10.1007/978-94-011-1870-5, URL http://link.springer.com/10.1007/978-94-011-1870-5.

[9] Woltman, S. J., Jay, G. D., and Crawford, G. P., "Liquid-crystal materials find a new order in biomedical applications," *Nature Materials*, Vol. 6, No. 12, 2007, pp. 929–938. https://doi.org/10.1038/nmat2010.

[10] Hao, T., "Electrorheological Fluids," *Advanced Materials*, Vol. 13, No. 24, 2001, pp. 1847–1857. https://doi.org/10.1002/1521-4095(200112)13:24<1847::AID-ADMA1847>3.0.CO;2-A, URL https://onlinelibrary.wiley.com/doi/abs/10.1002/1521-4095%28200112%2913%3A24%3C1847%3A%3AAID-ADMA1847%3E3.0.CO%3B2-A, _eprint: https://onlinelibrary.wiley.com/doi/pdf/10.1002/1521-4095%28200112%2913%3A24%3C1847%3A%3AAID-ADMA1847%3E3.0.CO%3B2-A.

[11] Hao, T., "The positive, negative, photo-ER, and electromagnetorheological (EMR) effects," *Studies in Interface Science*, Vol. 22, Elsevier, 2005, pp. 83–113. https://doi.org/10.1016/S1383-7303(05)80018-3, URL https://linkinghub.elsevier.com/retrieve/pii/S1383730305800183.

[12] Tao, R., "Electric-field-induced phase transition in electrorheological fluids," *Physical Review E*, Vol. 47, No. 1, 1993, pp. 423–426. https://doi.org/10.1103/PhysRevE.47.423, URL https://link.aps.org/doi/10.1103/PhysRevE.47.423, publisher: American Physical Society.

[13] Sadeghi, A., Beccai, L., and Mazzolai, B., "Innovative soft robots based on electro-rheological fluids," *2012 IEEE/RSJ International Conference on Intelligent Robots and Systems*, 2012, pp. 4237–4242. https://doi.org/10.1109/IROS.2012.6385846, iSSN: 2153-0866.

[14] Choi, S., Yook, J.-Y., Choi, M.-K., Nguyen, H., Lee, Y.-S., and Han, M.-S., "Speed Control of DC Motor using Electrorheological Brake System," *Journal of Intelligent Material Systems and Structures - J INTEL MAT SYST STRUCT*, Vol. 18, 2007, pp. 1191–1196. https://doi.org/10.1177/1045389X07083135.

[15] Stanway, R., Sproston, J. L., and El-Wahed, A. K., "Applications of electro-rheological fluids in vibration control: a survey," *Smart Materials and Structures*, Vol. 5, No. 4, 1996, p. 464. https://doi.org/10.1088/0964-1726/5/4/011, URL https://dx.doi.org/10.1088/0964-1726/5/4/011.

[16] Chu, J. H., and I, L., "Direct observation of Coulomb crystals and liquids in strongly coupled rf dusty plasmas," *Physical Review Letters*, Vol. 72, No. 25, 1994, pp. 4009–4012. https://doi.org/10.1103/PhysRevLett.72.4009, URL https://link.aps.org/doi/10.1103/PhysRevLett.72.4009, publisher: American Physical Society.

[17] Thomas, H., Morfill, G. E., Demmel, V., Goree, J., Feuerbacher, B., and Möhlmann, D., "Plasma Crystal: Coulomb Crystallization in a Dusty Plasma," *Physical Review Letters*, Vol. 73, No. 5, 1994, pp. 652–655. https://doi.org/10.1103/PhysRevLett.73.652, URL https://link.aps.org/doi/10.1103/PhysRevLett.73.652, publisher: American Physical Society.

[18] Nefedov, A., Petrov, O., Molotkov, V., and Fortov, V., "Formation of liquidlike and crystalline structures in dusty plasmas," *IEEE Transactions on Plasma Science*, Vol. 29, No. 2, 2001, pp. 210–215. https://doi.org/10.1109/27.923696, conference Name: IEEE Transactions on Plasma Science.

[19] Hartmann, P., Douglass, A., Reyes, J. C., Matthews, L. S., Hyde, T. W., Kovács, A., and Donkó, Z., "Crystallization Dynamics of a Single Layer Complex Plasma," *Physical Review Letters*, Vol. 105, No. 11, 2010, p. 115004. https://doi.org/10.1103/PhysRevLett.105.115004, URL https://link.aps.org/doi/10.1103/PhysRevLett.105.115004, publisher: American Physical Society.

[20] Molotkov, V. I., Nefedov, A. P., Pustyl'nik, M. Y., Torchinsky, V. M., Fortov, V. E., Khrapak, A. G., and Yoshino, K., "Liquid plasma crystal: Coulomb crystallization of cylindrical macroscopic grains in a gas-discharge plasma," *Journal of Experimental and Theoretical Physics Letters*, Vol. 71, No. 3, 2000, pp. 102–105. https://doi.org/10.1134/1.568290, URL https://doi.org/10.1134/1.568290.

[21] Banu, N., and Ticoş, C. M., "Precession of cylindrical dust particles in the plasma sheath," *Physics of Plasmas*, Vol. 22, No. 10, 2015, p. 103704. https://doi.org/10.1063/1.4933032, URL https://aip.scitation.org/doi/10.1063/1.4933032, publisher: American Institute of Physics.

[22] Fortov, V. E., Nefedov, A. P., Molotkov, V. I., Petrov, O. F., Poustylnik, M. Y., Torchinsky, V. M., and Khrapak, A. G., "Dusty plasmas in a dc glow discharge," *AIP Conference Proceedings*, Vol. 649, No. 1, 2002, pp. 394–397. https://doi.org/10.1063/1.1527807, URL https://aip.scitation.org/doi/abs/10.1063/1.1527807, publisher: American Institute of Physics.

[23] Khrapak, A., Molotkov, V., Nefedov, A., Torchinsky, V., and Yoshino, K., "Liquid and crystalline structures in dusty plasmas: dust liquid crystal," *Proceedings of 1999 IEEE 13th International Conference on Dielectric Liquids (ICDL'99) (Cat. No.99CH36213)*, 1999, pp. 657–660. https://doi.org/10.1109/ICDL.1999.799021.

[24] Ivlev, A. V., Morfill, G. E., Thomas, H. M., Räth, C., Joyce, G., Huber, P., Kompaneets, R., Fortov, V. E., Lipaev, A. M., Molotkov, V. I., Reiter, T., Turin, M., and Vinogradov, P., "First Observation of Electrorheological Plasmas," *Physical Review Letters*, Vol. 100, No. 9, 2008, p. 095003. https://doi.org/10.1103/PhysRevLett.100.095003, URL https://link.aps.org/doi/10.1103/PhysRevLett.100.095003, publisher: American Physical Society.

[25] Ivlev, A. V., Brandt, P. C., Morfill, G. E., Rath, C., Thomas, H. M., Joyce, G., Fortov, V. E., Lipaev, A. M., Molotkov, V. I., and Petrov, O. F., "Electrorheological Complex Plasmas," *IEEE Transactions on Plasma Science*, Vol. 38, No. 4, 2010, pp. 733–740. https://doi.org/10.1109/TPS.2009.2037716, conference Name: IEEE Transactions on Plasma Science.

[26] Dietz, C., Budak, J., Kamprich, T., Kretschmer, M., and Thoma, M. H., "Phase transition in electrorheological plasmas," *Contributions to Plasma Physics*, Vol. 61, No. 10, 2021, p. e202100079. https://doi.org/10.1002/ctpp.202100079, URL https://onlinelibrary.wiley.com/doi/abs/10.1002/ctpp.202100079, _eprint: https://onlinelibrary.wiley.com/doi/pdf/10.1002/ctpp.202100079.

[27] Thomas, H. M., Morfill, G. E., Fortov, V. E., Ivlev, A. V., Molotkov, V. I., Lipaev, A. M., Hagl, T., Rothermel, H., Khrapak, S. A., Suetterlin, R. K., Rubin-Zuzic, M., Petrov, O. F., Tokarev, V. I., and Krikalev, S. K., "Complex plasma laboratory PK-3 Plus on the International Space Station," *New Journal of Physics*, Vol. 10, No. 3, 2008, p. 033036. https://doi.org/10.1088/1367-2630/10/3/033036, URL https://dx.doi.org/10.1088/1367-2630/10/3/033036.

[28] Kompaneets, R., Morfill, G. E., and Ivlev, A. V., "Design of new binary interaction classes in complex plasmas," *Physics of Plasmas*, Vol. 16, No. 4, 2009, p. 043705. https://doi.org/10.1063/1.3112703, URL http://aip.scitation.org/doi/10.1063/1.3112703.

[29] Ivlev, A. V., Thoma, M. H., Räth, C., Joyce, G., and Morfill, G. E., "Complex plasmas in external fields: the role of non-hamiltonian interactions," *Physical Review Letters*, Vol. 106, No. 15, 2011, p. 155001. https://doi.org/10.1103/PhysRevLett.106.155001.

[30] Vermillion, K., Sanford, D., Matthews, L., Hartmann, P., Rosenberg, M., Kostadinova, E., Carmona-Reyes, J., Hyde, T., Lipaev, A. M., Usachev, A. D., Zobnin, A. V., Petrov, O. F., Thoma, M. H., Pustylnik, M. Y., Thomas, H. M., and Ovchinin, A., "Influence of temporal variations in plasma conditions on the electric potential near self-organized dust chains," *Physics of Plasmas*, Vol. 29, No. 2, 2022, p. 023701. https://doi.org/10.1063/5.0075261, URL https://aip.scitation.org/doi/10.1063/5.0075261, publisher: American Institute of Physics.

[31] Matthews, L. S., Vermillion, K., Hartmann, P., Rosenberg, M., Rostami, S., Kostadinova, E. G., Hyde, T. W., Pustylnik, M. Y., Lipaev, A. M., Usachev, A. D., Zobnin, A. V., Thoma, M. H., Petrov, O. F., Thomas, H. M., and Novitskiy, O. V., "Effect of ionization waves on dust chain formation in a DC discharge," *Journal of Plasma Physics*, Vol. 87, No. 6, 2021, p. 905870618. https://doi.org/10.1017/S0022377821001215, URL https://www.cambridge.org/core/journals/journal-of-plasma-physics/article/abs/effect-of-ionization-waves-on-dust-chain-formation-in-a-dc-discharge/8C3DCAB12A6E62C9903CA7B0524004EE, publisher: Cambridge University Press.

[32] Hartmann, P., Rosenberg, M., Juhasz, Z., Matthews, L. S., Sanford, D. L., Vermillion, K., Carmona-Reyes, J., and Hyde, T. W., "Ionization waves in the PK-4 direct current neon discharge," *Plasma Sources Science and Technology*, Vol. 29, No. 11, 2020, p. 115014. https://doi.org/10.1088/1361-6595/abb955, URL https://dx.doi.org/10.1088/1361-6595/abb955, publisher: IOP Publishing.

[33] Kostadinova, E. G., Busse, K., Liaw, C. D., Matthews, L. S., and Hyde, T. W., "Nematic transition in microgravity complex plasma liquid crystals," , ???? Presented at the 15th Dusty Plasma Workshop, Baltimore, Maryland, USA, Jun. 2018. [Online]. Available: https://wpdp.umbc.edu/files/2017/09/15DPW_Booklet_v03.pdf.

[34] Mitic, S., Pustylnik, M. Y., Erdle, D., Lipaev, A. M., Usachev, A. D., Zobnin, A. V., Thoma, M. H., Thomas, H. M., Petrov, O. F., Fortov, V. E., and Kononenko, O., "Long-term evolution of the three-dimensional structure of string-fluid complex plasmas in the PK-4 experiment," *Physical Review E*, Vol. 103, No. 6, 2021, p. 063212. https://doi.org/10.1103/PhysRevE.103.063212, URL https://link.aps.org/doi/10.1103/PhysRevE.103.063212, publisher: American Physical Society.

[35] Pustylnik, M. Y., Klumov, B., Rubin-Zuzic, M., Lipaev, A. M., Nosenko, V., Erdle, D., Usachev, A. D., Zobnin, A. V., Molotkov, V. I., Joyce, G., Thomas, H. M., Thoma, M. H., Petrov, O. F., Fortov, V. E., and Kononenko, O., "Three-dimensional structure of a string-fluid complex plasma," *Physical Review Research*, Vol. 2, No. 3, 2020, p. 033314. https://doi.org/10.1103/PhysRevResearch.2.033314, URL https://link.aps.org/doi/10.1103/PhysRevResearch.2.033314.

[36] Yaroshenko, V., and Pustylnik, M., "Possible Mechanisms of String Formation in Complex Plasmas at Elevated Pressures," *Molecules*, Vol. 26, No. 2, 2021, p. 308. https://doi.org/10.3390/molecules26020308, URL https://www.mdpi.com/1420-3049/26/2/308, number: 2 Publisher: Multidisciplinary Digital Publishing Institute.

[37] Takahashi, K., Tonouchi, M., Adachi, S., and Totsuji, H., "Study of Cylindrical Dusty Plasmas in PK-4J; Experiments," Vol. 31, No. 2, 2014, p. 4.

[38] Totsuji, H., Totsuji, C., Takahashi, K., and Adachi, S., "Study of Cylindrical Dusty Plasmas in PK-4J; Theory and Simulations," Vol. 31, No. 2, 2014, p. 7.

[39] Pustylnik, M. Y., Fink, M. A., Nosenko, V., Antonova, T., Hagl, T., Thomas, H. M., Zobnin, A. V., Lipaev, A. M., Usachev, A. D., Molotkov, V. I., Petrov, O. F., Fortov, V. E., Rau, C., Deysenroth, C., Albrecht, S., Kretschmer, M., Thoma, M. H., Morfill, G. E., Seurig, R., Stettner, A., Alyamovskaya, V. A., Orr, A., Kufner, E., Lavrenko, E. G., Padalka, G. I., Serova, E. O., Samokutyayev, A. M., and Christoforetti, S., "Plasmakristall-4: New complex (dusty) plasma laboratory on board the International Space Station," *The Review of Scientific Instruments*, Vol. 87, No. 9, 2016, p. 093505. https://doi.org/10.1063/1.4962696.

[40] Kim, Y. H., Lee, J.-O., Jeong, H. S., Kim, J. H., Yoon, E. K., Yoon, D. K., Yoon, J.-B., and Jung, H.-T., "Optically selective microlens photomasks using self-assembled smectic liquid crystal defect arrays," *Advanced Materials (Deerfield Beach, Fla.)*, Vol. 22, No. 22, 2010, pp. 2416–2420. https://doi.org/10.1002/adma.200903728.

[41] Son, B., Kim, S., Kim, Y. H., Käläntär, K., Kim, H.-M., Jeong, H.-S., Choi, S. Q., Shin, J., Jung, H.-T., and Lee, Y.-H., "Optical vortex arrays from smectic liquid crystals," *Optics Express*, Vol. 22, No. 4, 2014, pp. 4699–4704. https://doi.org/10.1364/OE.22.004699, URL https://opg.optica.org/oe/abstract.cfm?uri=oe-22-4-4699, publisher: Optica Publishing Group.

[42] Coursault, D., Blach, J.-F., Grand, J., Coati, A., Vlad, A., Zappone, B., Babonneau, D., Lévi, G., Félidj, N., Donnio, B., Gallani, J.-L., Alba, M., Garreau, Y., Borensztein, Y., Goldmann, M., and Lacaze, E., "Tailoring Anisotropic Interactions between Soft Nanospheres Using Dense Arrays of Smectic Liquid Crystal Edge Dislocations," *ACS nano*, Vol. 9, No. 12, 2015, pp. 11678–11689. https://doi.org/10.1021/acsnano.5b02538.

[43] Gryn, I., Lacaze, E., Carbone, L., Giocondo, M., and Zappone, B., "Electric-Field-Controlled Alignment of Rod-Shaped Fluorescent Nanocrystals in Smectic Liquid Crystal Defect Arrays," *Advanced Functional Materials*, Vol. 26, 2016. https://doi.org/10.1002/adfm.201602729.

[44] Nefedov, A. P., Morfill, G. E., Fortov, V. E., Thomas, H. M., Rothermel, H., Hagl, T., Ivlev, A. V., Zuzic, M., Klumov, B. A., Lipaev, A. M., Molotkov, V. I., Petrov, O. F., Gidzenko, Y. P., Krikalev, S. K., Shepherd, W., Ivanov, A. I., Roth, M., Binnenbruck, H., Goree, J. A., and Semenov, Y. P., "PKE-Nefedov*: plasma crystal experiments on the International Space Station," *New Journal of Physics*, Vol. 5, No. 1, 2003, p. 33. https://doi.org/10.1088/1367-2630/5/1/333, URL https://dx.doi.org/10.1088/1367-2630/5/1/333.

[45] Nitter, T., "Levitation of dust in rf and dc glow discharges," *Plasma Sources Science and Technology*, Vol. 5, No. 1, 1996, p. 93. https://doi.org/10.1088/0963-0252/5/1/012, URL https://dx.doi.org/10.1088/0963-0252/5/1/012.

[46] Fortov, V. E., Ivlev, A. V., Khrapak, S. A., Khrapak, A. G., and Morfill, G. E., "Complex (dusty) plasmas: Current status, open issues, perspectives," *Physics Reports*, Vol. 421, 2005, pp. 1–103. https://doi.org/10.1016/j.physrep.2005.08.007, URL https://ui.adsabs.harvard.edu/abs/2005PhR...421....1F, aDS Bibcode: 2005PhR...421....1F.